Investigation of Orifice Compliance Effects on Steady-State Pressure Gradient in Replacement Heart Valves

Kevin R. Anderson [1],

ABSTRACT

Replacement heart valves were first developed in the 1950's and advancements to these medical devices continue to be verified with extensive in vitro flow testing. Test valves are traditionally mounted on durometer shore hardness 60A silicone rubber gaskets to facilitate fixturing in various test apparatuses, however the impact of this material hardness selection has not been studied with respect to hydrodyanmic performance. This investigation assesses the effects of durometer shore hardness, by evaluating the pressure drop across compliant orifices under steady-state flow conditions. Geometrically identical gaskets were constructed from durometer shore hardness 10A, 20A, 40A, 60A, and 90A materials. The pressure drop across each of these test specimens was evaluated with a steady flowrate of 20L/min using experimental techniques and computer models. The results indicate that no significant difference in pressure drop occurred among the 60A and 90A specimens. However, reducing the durometer shore hardness to 40A, 20A, and 10A did have a significant impact on orifice pressure drop.

Keywords: cardiology diagnostic tests, ventricular conductance volume, ventricular blood pressure, catheterization techniques, and pressure-volume loop analysis

1. INTRODUCTION

Cardiovascular disease is currently the leading cause of death in the United States and diseased heart valves are a key contributor to this statistic [1]. Modeling and experimental efforts in the aortic region of the heart are proliferate in the literature. The work of [2] presents a theoretical model of the transient viscous blood flow across the aortic stenosis is derived by taking into account the aorta compliance. The relation was evaluated using clinical values of pressure drops for cases witnessing low flow and low gradient aortic stenosis (AS). In the work of [3] a lumped parameter model, solely based on non-invasive data, allowing the description of the interaction between left ventricle (LV), coarctation of the aorta (COA), AS and the arterial system is presented. In the research of [4] numerical and experimental investigations of pulsatile blood flow patterns through a dysfunctional mechanical heart valve are presented. The experiments of [5] time-resolved PIV measurements of the flow field in a stenosed, compliant arterial model are presented. Compliant (flexible) structures play an important role in several biological flows including the lungs, heart and arteries. To study these problems experimentally in vitro, especially using flow visualization techniques, can be expensive due to the high-intensity and high-repetition rate light sources required. The work of [6] gives an overview of recent advances in computational methodologies for the simulation of mechanical circulatory assist devices. The study of [7] affords a roadmap for implementing boundary conditions in simulations of arterial flows. In the study of [8] FluidStructure Interaction (FSI) Simulation of pulsatile ventricular assist devices is given. The modeling o the instantaneous pressure gradient across the aortic valve is the subject of [9]. In the work of [10] the authors present mechanical behavior and computational simulation results for bioprosthetic heart valve. The flow in a bileaflet heart valve is the focus of the numerical and experimental based study of [11]. The work of [12] gives an overview of the state-of-the-art in prosthetic aortic heart valves modeling and design advances. Thus, this area of research is seen to be active. The particular merit of the present study is that is a combined numerical / experimental study which can be used to ascertain the impacts of compliant materials in the prosetic heart valves.

Replacement heart valve therapies have been developed since the 1950s to address this problem, evolving from mechanical ball and cage valves to tissue prostheses seen in Figure 1 and 2.

Improvements to these devices continue to be made and verified with rigorous *in vitro* experimental testing. To conduct such tests, specimens are mounted to shore 60A silicone rubber gaskets to facilitate fixturing in various test apparatuses. Recently a proposal to mount the valves on rigid gaskets, machined with evenly distributed attachment holes, has been made. This improvement would make the valve mounting process more consistent and easier, however the differences in gasket compliance have yet to be assessed. The focus of this study seeks to address this issue by investigating the impact of gasket compliance under steady-state flow conditions. Durometer is a common way of characterizing compliance of silicone rubber

Manuscript received on June 9, 2015 ; revised on December 12, 2015.

[1] Mechanical Engineering Department, California State Polytechnic University, Pomona, USA

Fig.1:: Starr-edwards ailastic ball valve aortic, model 1260.

Fig.2:: Carpentier-edwards aortic bioprosthesis, model 3000TFX.

materials. This property describes how resistant a material is to indentation from impact loading and is largely dependent upon the material's elastic modulus [13]. Durometer ratings are assigned to materials based on indentation results, where the durometer hardness rating is linearly related to the applied load required to reach a specified penetration depth [13, 14]. Thus, as durometer increases the stiffness of the material also increases. There are various durometer scales used to characterize compliant materials, but for the relevance of this study only materials with shore A rating are investigated

2. EXPERIMENTAL APPARATUS

All Test specimens of durometer shore hardness 10A, 20A, 40A, 60A, and 90A were die cut from 0.0625 inch thick sheets into 20 mm ID by 50 mm OD gaskets. An inner diameter of 20 mm was selected for the gaskets because this dimension is most appropriate for testing the smallest sized or worst-case prosthetic heart valves. Each specimen was made from silicone rubber except for the shore hardness 90A sample, which had to be constructed from polyurethane because of availability. Figure 3 shows each of the gaskets.

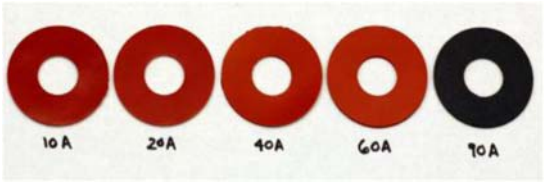

Fig.3:: Test specimens.

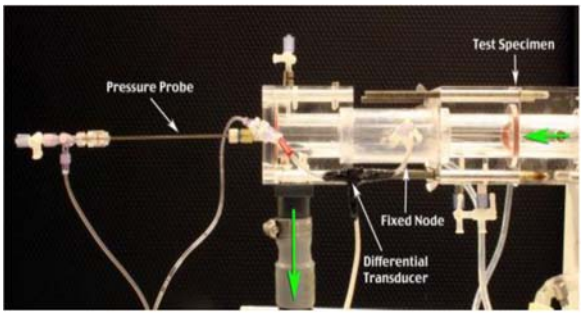

Fig.4:: Test apparatus.

Steady state testing was conducted on the gasket alone (without a prosthetic heart valve mounted to it) in a 35mm diameter flow chamber. A 0.9% saline solution was pumped at flow rate of 20L/min to simulate the steady state conditions. This flow rate was chosen because it is analogous to the time integrated flow experienced by a heart valve under normal physiologically 5L/min pulsatile conditions at 70 beats/min [15]. Thus, 20L/min represents theoretical steady-state physiologically conditions. Pressure measurements were acquired with a Honeywell differential transducer rated at 5 psi (Ref #26PCBFA6D) and an Endevco amplifier (Model 136). The differential transducer was attached to a pressure probe and a reference fixed node on the flow chamber so that measurements could be taken through the centerline of the test chamber and test specimen in the axial direction. Figure 4 diagrams the test apparatus.

Pressure measurements were taken through the centerline of the valve starting upstream and incrementally moving downstream. This was accomplished by marking a reference point on the moving pressure probe and incrementally moving it 0.25 inches axially. Flow was established with a centrifuge pump and measured with a calibrated Fischer & Porter Rotameter (Model 10A4555). To calculate the error associated with this experimental setup, the error in pipe diameters, differential transducer, and rotameter must be considered. Uncertainty in the amplifier, viscosity, and density were assumed small enough to be negligible. Thus, the overall uncertainty in the pressure measurements can be calculated from the Bernoulli Equation (neglecting frictional drops) and the Incompressible form of Conservation of Mass

as follows:

$$p_1 + \frac{1}{2}\rho V_1^2 = p_2 + \frac{1}{2}\rho V_2^2 \quad (1)$$

$$\Delta p = p_1 - p_2 = \frac{1}{2}\rho\left(V_2^2 - V_1^2\right) \quad (2)$$

$$Q = A_1 V_1 = A_2 V_2 = \frac{\pi}{4}D_1^2 V_1 = \frac{\pi}{4}D_2^2 V_2 \quad (3)$$

Thus, solving for the pressure drop

$$\Delta p = \left(\frac{1}{D_2^4 - D_1^4}\right)\left(\frac{8Q^2\rho}{\pi^2}\right) \quad (4)$$

Thus, following the methods of [16], the sensitivity is

$$\frac{\partial \Delta p}{\Delta p} = \pm\sqrt{\left(\frac{5\partial D_2}{D_2}\right)^2 + \left(\frac{5\partial D_1}{D_1}\right)^2 + \left(\frac{2\partial Q}{Q}\right)^2 + e^{2_{tr}}} \quad (5)$$

Given from the manufacture specifications, instrumentation error, and test apparatus geometry: D_1 = 35 mm,∂D_1 = 0.02 mm, D_2 = 20 mm, ∂D_2 = 0.02 mm, ∂Q/Q = 1%. The transducer error is taken as e_{tr} = 2% and the maximum Δp = 20 mm Hg. The uncertainty in differential pressure measurements becomes $\partial\Delta$p = $\pm$0.58 mm Hg or $\partial\Delta$p/Δp = 2.9%. This experimental error in pressure seems reasonable since the difference between the worst-case and best-case gasket are expected to be approximately 5 mmHg. Thus, the experimental apparatus can successfully enable the distinction of test specimens based on differential pressure.

3. CFD MODELING

In addition to acquiring pressure data, profiles of the gaskets were photographed within the test chamber. These images were then digitized into Cartesian coordinates with the NIH's public image library [17]. From this data, 3D geometries were constructed and Computational Fluid Dynamics (CFD) models meshed using polyhedral cells. Prism cells were also used, but only at the walls of the model. Furthermore, refinements were made around the specimen surface to give a finer mesh in this critical region. This resulted in meshes with approximately 90,000 to 100,000 cells. An isometric view of the shore hardness 10A specimen model is show in Figure **Error! Reference source not found**. as an illustrative example.

A zoomed in view of each mesh is diagramed in Figure **Error! Reference source not found.** with planar cross-sections of the 3D geometry compared to the pictures of the gaskets acquired at a flow rate of 20L/min. A CFD analysis was performed on each of the meshes shown in Figure **Error! Reference source not found.** using STAR CCM+. This is commercially available software that utilizes a Finite

Fig.5:: CFD model mesh, isometric view (shore hardness 10A model shown).

Volume solver. Each model was setup with an inlet velocity boundary condition of 0.346 m/s (average velocity in a 35mm tube with a volumetric flow rate of 20L/min) and standard outlet. A 0.9% saline solution is composed of water and salt. Since the salt contribution is small, it has little impact on the density and viscosity of the solution. Therefore, water can be selected to represent the fluid domain of the CFD models. Specifically, a density of a density of 998 kg/m^3 and viscosity of 889 $\times 10^{-6}$ kg/s-m were applied to represent water.

Given these boundary conditions and material properties, the Reynolds number for this problem can be calculated [8,10]: Re = ρVD/μ=13,600. A Reynolds number in excess of 2400 gives rise to turbulent flow in a pipe [18]. Thus, the default k-ϵ turbulence model was applied for all of the CFD simulations. CFD model validation was performed by comparison to calculated pressure drops from published orifice discharge coefficient data. Orifice discharge coefficients take into account the complexity of turbulence and viscous effects by relating them to idealized values governed by the Bernoulli's equation [18,19].

$$Q = C_d Q_{ideal} = C_d A_1 V_1 \quad (6)$$

$$Q = C_d\sqrt{\frac{\Delta p\pi}{8\rho\left(\frac{1}{D_2^4} - \frac{1}{D_1^4}\right)}} \quad (7)$$

And the pressure drop is taken from Eqn. (4). In order to determine the discharge coefficient C_d of a straight orifice, the Reynolds number and the ratio of tube to gasket diameter must be calculated. Recall that the Reynolds number was found to be 13,600 and the ratio of diameters is 20mm/35mm = 0.57. Thus, a discharge coefficient of 0.625 can be assumed from published straight orifice data with pressure taps at one diameter upstream and a half a diameter downstream [18]. The resulting pressure drop is then Δp=9.63 mm Hg.

The shore hardness 90A specimen represents a similar straight orifice to those investigated in the published discharge coefficient studies [20,21]. Thus, this

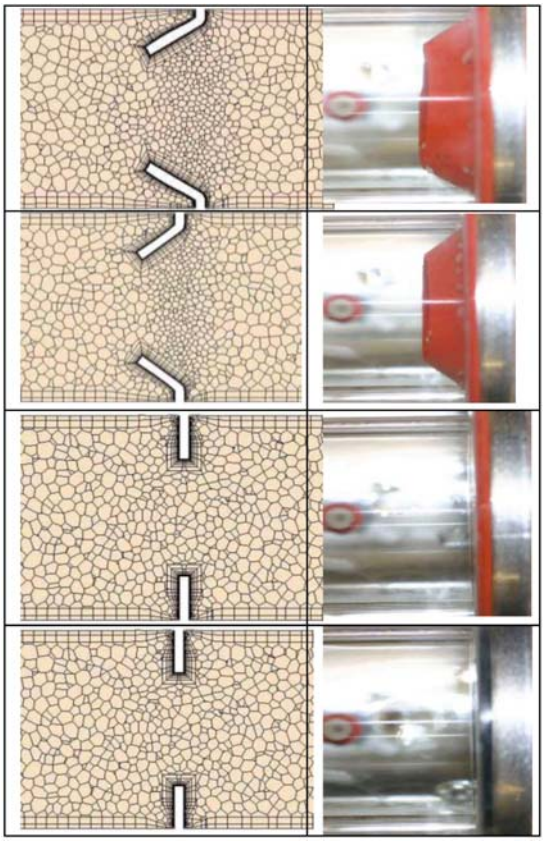

Fig. 6:: Computer models and pictures of shore hardness 10A, 20A, 40A, 60A, and 90A test specimens at 20L/min (from top to bottom).

model was run and a pressure drop of $\Delta p = 9.33$ mmHg was found across pressure taps at one diameter upstream and half a diameter downstream. Comparing these results, a 3.1% difference exists between the shore hardness 90A CFD model and the published straight orifice discharge coefficient data. Since this percent difference is less than 10%, it is reasonable to assume that the modeling techniques used for each simulation are valid.

Finally, a mesh sensitivity study was preformed prior to running the shore hardness 10A, 20A, 40A, 60A, and 90A CFD simulations. Because the deformation exhibited by the durometer 10A test specimen is the more dramatic (referring to Figure **Error! Reference source not found.**), this CFD model was expected to be more dependent on mesh density. Therefore, the shore hardness 10A model is used as an illustrative example to investigate the dependence of pressure drop on mesh density for both hexahedral and polyhedral cells. Figure **Error! Reference source not found.** and **Error! Reference source not found.** diagram course and fine meshes evaluated while Figure **Error! Reference source not found.** summarizes the results with respect to a log scale of cell quantity.

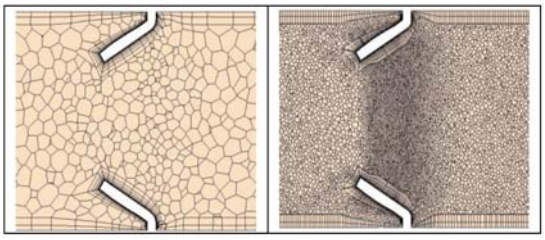

Fig. 7:: Polyhedral cell mesh (36,746 cells on left and 2,221,973 cells on the right).

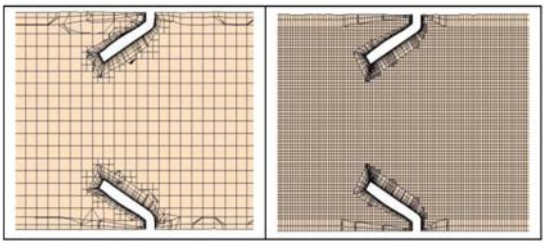

Fig. 8:: Hexahedral cell mesh (80,882 cells on left and 1,959,374 cells on the right).

In figure 9, note that pressure gradient across the gasket is independent of mesh density especially for meshes containing more than 90,000 cells. Furthermore, polyhedral and hexahedral cell meshes resulted in consistent solutions between 5.0 to 5.5 mmHg regardless of base shape. Since polyhedral cells converge faster on a solution than hexahedral cells these are preferred to reduce computational time. Therefore, polyhedral meshes with approximately 90,000-100,000 cells are appropriate for the durometer 10A, 20A, 40A, 60A, and 90A CFD models.

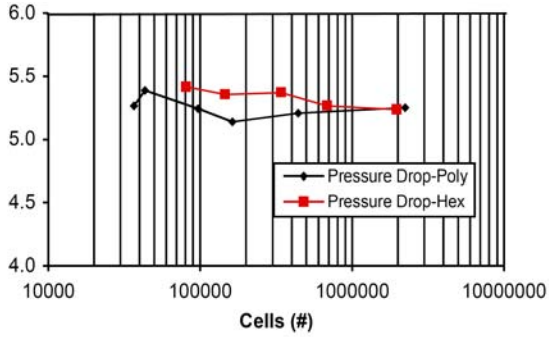

Fig. 9:: Pressure gradient dependence on mesh density.

4. RESULTS

Comparing the experimental pressure data among the gasket specimens, those with higher durometer ratings exhibited higher pressures. This is to be expected since the stiffer the gasket the more resistant it is to the flow. Furthermore, a stiffer gasket is less likely to expand beyond its fabricated 20mm ID, increasing its orifice area, and thereby decreasing the pressure drop. Figure **Error! Reference source not found.** illustrates the pressure data collected for test specimens of durometer shore hardness 10A, 20A, 40A, 60A, and 90A.

Note the characteristic pressure dip and recovery for each of the gaskets. The 40A, 60A, and 90A specimens all behaved similarly with comparably larger pressure drops with respect to the 10A and 20A specimens. Figure **Error! Reference source not found.** illustrates the significance of these differences by presenting the overall pressure drop (the extreme inflow pressure minus the extreme outflow pressure) for each gasket with measurement error calculated as previously outlined in this paper.

Clearly, the 10A and 20A have a significant difference in pressure drop when compared to the stiffer gaskets. Geometric observations of the gaskets under steady state conditions of 20L/min also give insight into these pressure results upon review each of the test specimens. For the 10A and 20A gaskets it is evident that deformation occurs, pushing the gasket downstream and away from central flow. This phenomenon allows the inner diameter to stretch to a larger size, decreasing the overall pressure drop by increasing the geometric orifice area and expending kinetic energy on the gasket deformation. It is interesting to note that the 40A specimen also deforms but this deformation causes the orifice to restrict from an ID of 20mm to an ID of 19.2 mm, thereby resulting in a greater pressure gradient. The CFD results show a similar trend to the experimental findings. The pressure gradients of these computer simulations are summarized in Figure 11. The computer models overestimate the experimental results for the durometer 10A, 20A, and 40A while underestimating the 60A and 90A pressure gradients. Regardless, both the experimental and modeled results show similar trends in dependence of pressure drop on durometer. Increases in stiffness from 60A to 90A have little impact on pressure gradient, while increases in stiffness from 10A to 40A significantly contribute to greater pressure gradients. Contour plots of these pressure gradients and corresponding velocity magnitudes are presented in Figure 12 and Figure 13 for durometer 10A, Figure 14 and Figure 15 for durometer 20A, Figure 16 and Figure 17 for durometer 40A, Figure 18 and Figure 19 for durometer 60A and Figure 20 and Figure 21 for durometer 90A, respectively. The results shown in Figure 12 through Figure 21 are seen to be in qualitative agreement with those of [22].

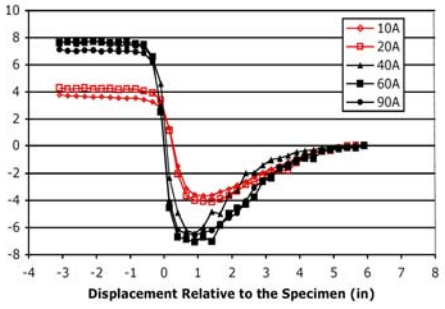

Fig.10:: Experimental pressure data (0 inch displacement represents the outflow edge of the test specimen).

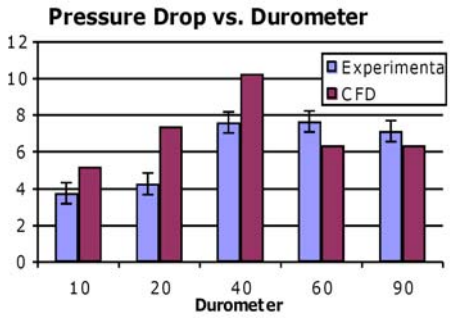

Fig.11:: Experimental pressure drop vs. durometer.

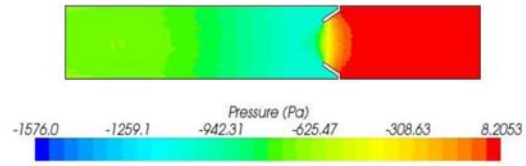

Fig.12:: Pressure contour, durometer 10A model.

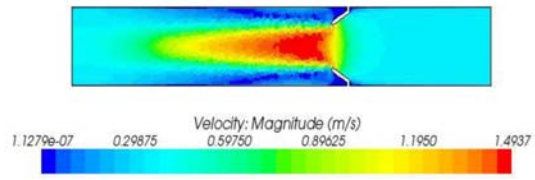

Fig.13:: Velocity magnitude contour, durometer 10A model.

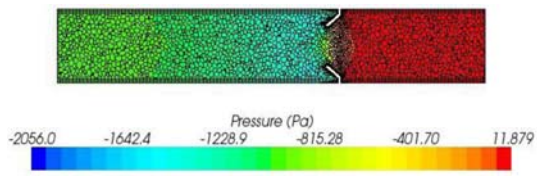

Fig.14:: Pressure contour, durometer 20A model.

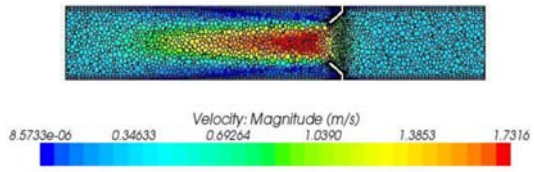

Fig.15:: Velocity magnitude contour, durometer 20A model.

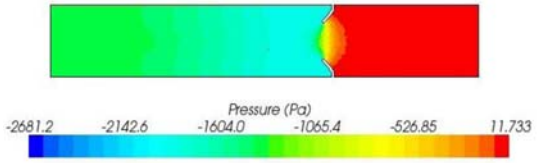

Fig.16:: Pressure contour, durometer 40A model.

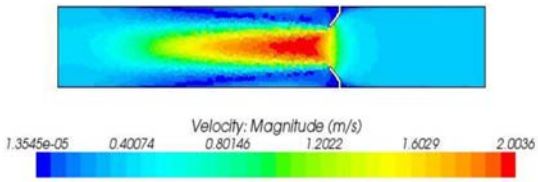

Fig.17:: Velocity magnitude contour, durometer 40A model.

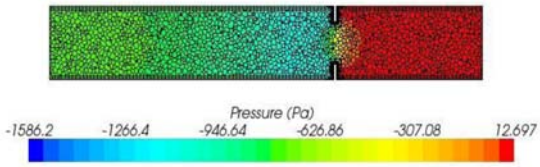

Fig.18:: Pressure contour, durometer 60A model.

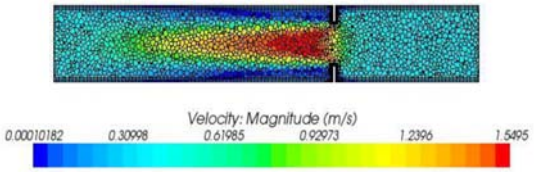

Fig.19:: Velocity magnitude contour, durometer 60A model.

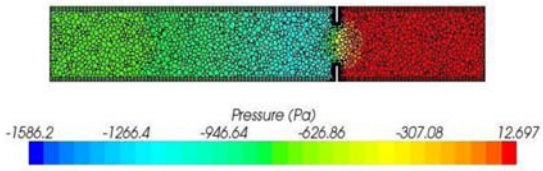

Fig.20:: Pressure Contour, Durometer 90A Model.

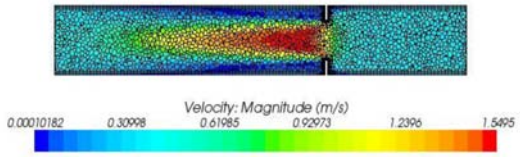

Fig.21:: Velocity magnitude contour, durometer 90A model.

5. CONCLUSIONS

The focus of this paper seeks to address this issue by investigating the impact of heart valve gasket compliance under steady-state flow conditions. Durometer is a common way of characterizing compliance of silicone rubber materials. Experiments and numerical simulations have been carried out in prosthetic heart valve in order to quantify the effects of durometer shore hardness on hydrodynamic pressure drop performance. It has been found in this paper, that changing from a shore 60A gasket to a stiffer material would have an insignificant impact on steady-state pressure drop measurement as seen in the similarities between the shore 60A and 90A gaskets in the experimental and visually observed CFD results. Therefore, the proposal to switch to a rigid gasket for prosthetic heart valve is reasonable for steady-state testing. A continuation of this analysis should be performed to investigate the impact of gasket compliance under pulsating flow conditions. Perhaps, a replacement heart valve rigidly mounted would have premature opening and closing under these circumstances. Further research should focus on how these outcomes differ from physiological conditions as indicated in [23].

References

[1] A. Minino, M. Arialdi, M. P. Heron, and B. L. Smith. "Death: Preliminary Data for 2004," *National Vital Statistics Reports*, vol. 54, no. 19, pp. 1-50, 2006.

[2] H. Mohammadi, R. Cartier, and R. Mongrain, "Derivation of a Simplified Relation for Assessing Aortic Root Pressure Drop Incorporating Wall Compliance," *Medical & Biological Engineering & Computing*, vol.53, no. 3, pp. 241-251, 2015

[3] Z. Keshavarz-Motamed, J. Garcia, P. Pibarot, E. Larose, and L. Kadem, "Modeling the Impact of Concomitant Aortic Stenosis and Coarctation of the Aorta on Left Ventricular Workload," *Journal of Biomechanics*, vol. 44, no. 16, pp. 2817-2825, 2011.

[4] O. Smadi, "Numerical and Experimental Investigations of Pulsatile Blood Flow Pattern Through a Dysfunctional Mechanical Heart Valve," *Journal of Biomechanics*, vol. 43 no. 8, pp. 1565-1572, 2010.

[5] P. Geoghegan, N. Buchmann, J. Soria, and M. Jermy, "Time-resolved PIV Measurements of the

Flow Field in a Stenosed, Compliant Arterial Model," *Experiments in Fluids*. vol. 54, no. 5, pp. 1-19, 2013.

[6] A.L. Marsden, Y. Bazilevs, C.C. Long, and M. Behr, "Recent Advances in Computational Methodology for Simulation of Mechanical Circulatory Assist Devices," *Wiley Interdisciplinary Reviews-systems Biology and Medicine*, vol. 6, no. 2, pp. 169-188, 2014.

[7] J.M. Bokov, "Implementing Boundary Conditions in Simulations of Arterial Flows," *Journal of Biomechanical Engineering*, vol. 135, no. 11, pp. 111004-111009, 2013.

[8] C.C. Long, "Fluidstructure Interaction Simulation of Pulsatile Ventricular Assist Devices," *Computational Mechanics*, vol. 52 , no. 5, pp. 971-981, 2013.

[9] "Analytical Model Describes Instantaneous Pressure Gradient Across Aortic Valve," *World Disease Weekly*. 89. 2005.

[10] M.S. Sacks, "Bioprosthetic Heart Valve Heterograft Biomaterials: Structure, Mechanical Behavior and Computational Simulation," *Expert Review of Medical Devices*, vol. 3, no. 6, pp. 817-834, 2006.

[11] L. Ge, H.L. Leo, F. Sotiropoulos, and A.P. Yoganathan, "Flow in a Mechanical Bileaflet Heart Valve at Laminar and Near-peak Systole Flow Rates: CFD Simulations and Experiment,." *Journal of Biomechanical Engineering-Transactions of the ASME*, vol.127, no. 5, pp. 782-797, 2005.

[12] A. Kheradvar, E.M. Groves, C.J. Goergen, S. H. Alavi, R. Tranquillo, C. A. Simmons, L. P. Dasi, K. J. Grande-Allen, M. Mofrad, A. Falahatpisheh, B. Griffith, F. Baaijens, S. H. Little, and S. Canic, "Emerging Trends in Heart Valve Engineering: Part II. Novel and Standard Technologies for Aortic Valve Replacement," *Annals of Biomedical Engineering*, vol. 43, no. 4, pp. 844-857, 2015.

[13] F. Casa, M. Fenzi, and L. Tontodonati, "Study of Hardness Drift: A Method for Investigating the Viscous Behaviour of Cured Rubber," *Polymer Testing*, vol. 14, no. 4, pp. 355-367, 1995.

[14] D. Garcia, P. Pibarot, and L.G. Durand, "Analytical modeling of the instantaneous pressure gradient across the aortic valve," *Journal of Biomechanics*, vol. 38, pp. 1303-1311, 2005.

[15] D. Garcia, L. Kadem, D. Savery, P. Pibarot, and L.G. Durand, "Analytical modeling of the instantaneous maximal transvalvular pressure gradient in aortic stenosis," *Journal of Biomechanics*, vol.39, no. 16, pp. 3036-3044, 2006.

[16] J.R. Taylor, *An Introduction to Error Analysis: The Study of Uncertainties in Physical Measurements*, 2nd Ed., University Science Books, Sausalito, 1997, pp. 45-79.

[17] W.S. Rasband, U. S. National Institutes of Health, Bethesda, Maryland, USA, http://rsb.info.nih.gov/ij/, 1997-2006.

[18] R.L. Panton, *Incompressible Flow*, 3rd Ed. ,Wiley, New York, 2005.

[19] Measurement of Fluid Flow by Means of Orifice Plates, Nozzles, and Venturi Tubes Inserted in Circular Cross-Section Conduits Running Full. International Standard ISO 5167, 1980.

[20] M.I. Mohamed, and G. A. Aggag. "Uncertainty evaluation of shore hardness testers," *Measurement*, vol. 33, pp. 251-257, 2003.

[21] K. Ramamurthi and K. Nandakumar, "Characteristics of flow through small sharp-edged cylindrical orifices," *Flow Measurement and Instrumentation*, vol. 10, pp. 133-143, 1999.

[22] W.L. Lim, Y.T. Chew, T.C. Chew, and H.T. Low, "Steady flow dynamics of prosthetic aortic heart valves: a comparative evaluation with PIV techniques," *Journal of Biomechanics*, vol. 31, pp. 411-421, 1998.

[23] A. Vander, J. Sherman, and D. Luciano. *Human Physiology: The Mechanisms of Body Function*, 8th Ed., McGraw-Hill ,New York, 2001.

Kevin R. Anderson is a Professor of Mechanical Engineering at California State Polytechnic University at Pomona (Cal Poly Pomona). He received his BSME from Cal Poly in 1991, his MSME from CU Boulder in 1994, and his Ph.D. from CU Boulder in 1998 in the area of Combustion. Currently, he is the director of the solar thermal alternative renewable energy laboratory. He holds 20 years of consulting experience in the private sector of engineering. His publications are listed on www.csupomona.edu/ kranderson1 and his areas of expertise include thermal and fluid analysis, CFD simulation, machine design, control systems, and alternative/renewable energy technology development and design. He actively serves as editor, conference chair, and reviewer for various professional societies and journal publications. He can be contacted via his webpage at www.cpp.edu/ kranderson1.